A Microfluidics-Enabled Photonic Crystal Biosensor for Simplified, Point-of-Care Diagnosis of Blood Biomarker

Fuzhen Li[†a,b], Bin Shi[†*c], Zhijie Li[†d], Liang Huang[e], Yisilamu Yibulayimu[a,b], Yanlin Song[a,b], Zewei Lian[*f] and Meng Su[*a,b]

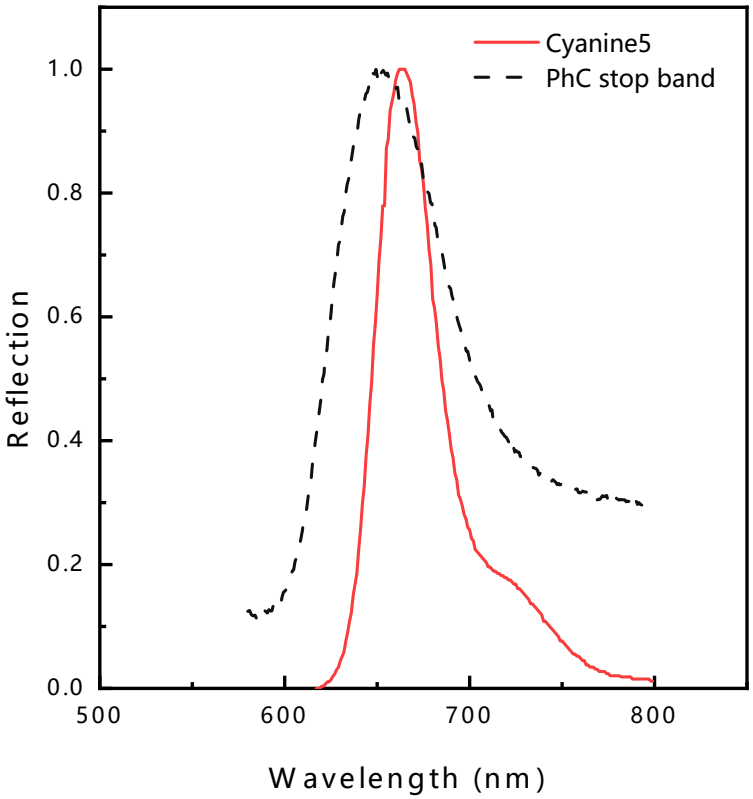

Figure S1. **Spectral matching of the emission to the photonic band edge.** The photonic stop band of the 290 nm self-assembled colloidal photonic crystal (colloidal PC), predicted by the Bragg–Snell relation and verified by reflection spectroscopy, is spectrally aligned with the Cy5 emission peak (~680 nm), enabling band-edge coupling and fluorescence enhancement through increased optical density of states.

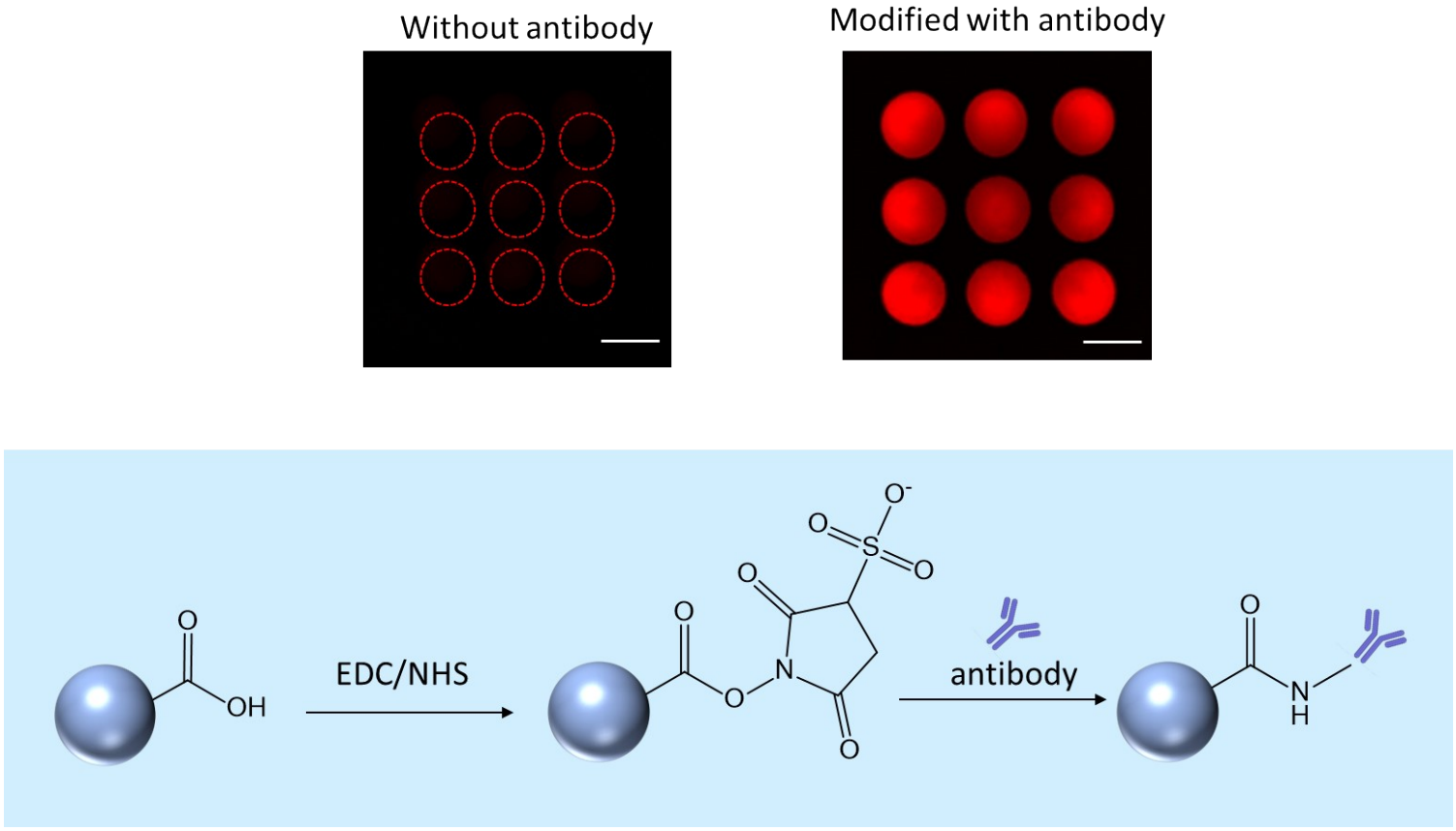

Figure S2. Modified PS photonic crystal with antibody. (a) Fluorescent images of PS arrays unmodified and modified with antibody. (b) Schematic of antibody functionalization on the colloidal photonic crystal surface.

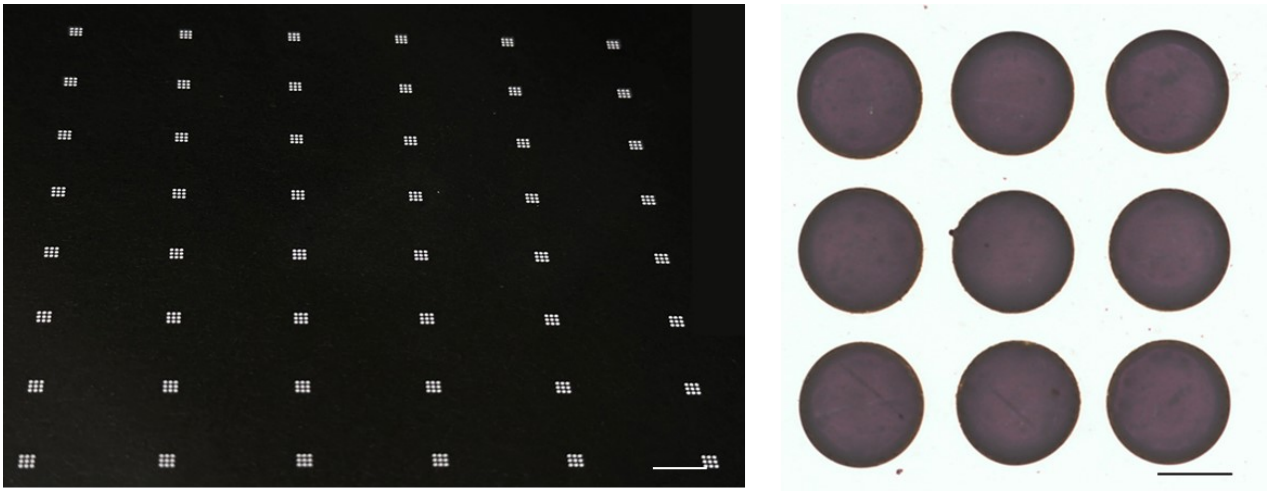

Figure S3. Large-area self-assembled colloidal photonic crystal chip. (a) Photograph of the fabricated large-area colloidal photonic crystal chip, showing uniform structural coloration across the large-area substrate. Scale bar: 5 mm. (b) Optical microscopy image of a PC unit. Scale bar: 500 μm.

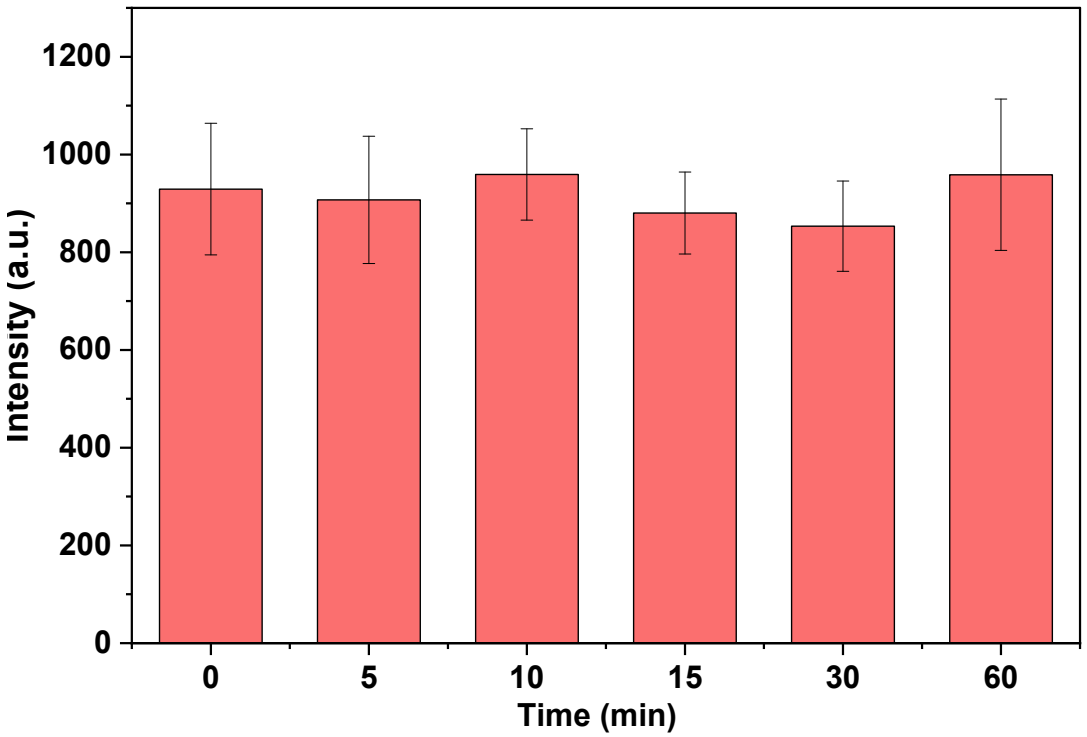

Figure S4. Fluorescence intensity of PC biochips after different times of storage away from light.

Time-dependent fluorescence intensity of the Cy5-labelled assay after standing for different durations. The fluorescence signal remains essentially unchanged over the tested time window, indicating good temporal stability and negligible signal degradation during the measurement process.

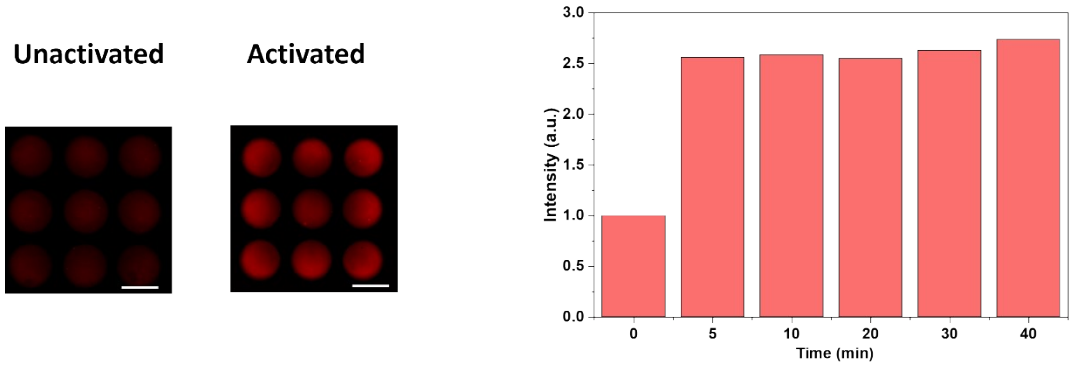

Figure S5. Optimization of the photonic crystal activation time. (a) Fluorescence images of colloidal photonic crystal arrays before and after surface activation.

(b) Quantitative fluorescence intensity of photonic crystal biochips as a function of activation duration. The results indicate that the fluorescence signal reaches saturation after an optimal activation period, providing guidance for consistent surface functionalization.

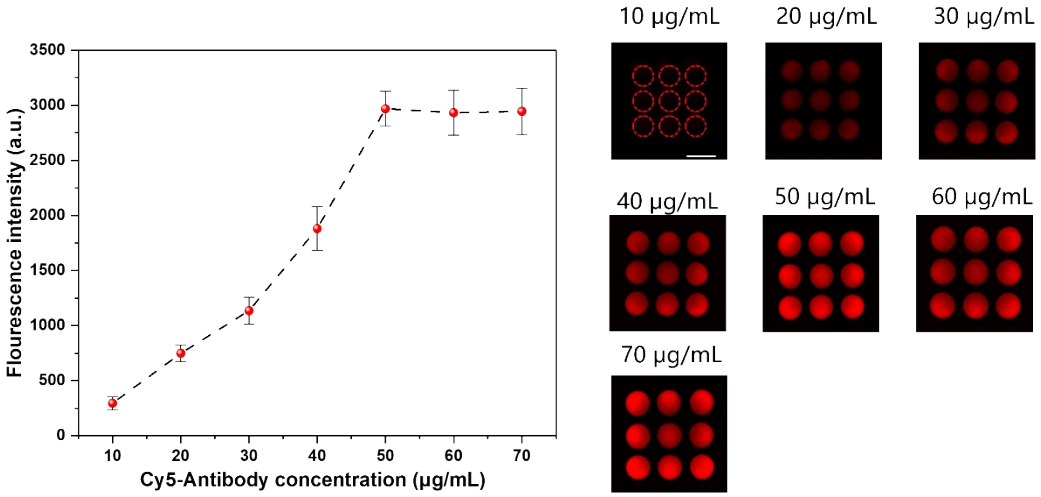

Figure S6. Optimization of surface antibody concentration on photonic crystal microspheres. (a) Scatter plot showing the quantitative fluorescence intensity of PC microspheres as a function of surface antibody concentration. (b) Fluorescence images of PC microsphere arrays functionalized with different antibody concentrations. Fluorescence intensity increases with antibody loading and reaches a plateau at 50 μg/mL, providing guidance for reproducible biochip functionalization.

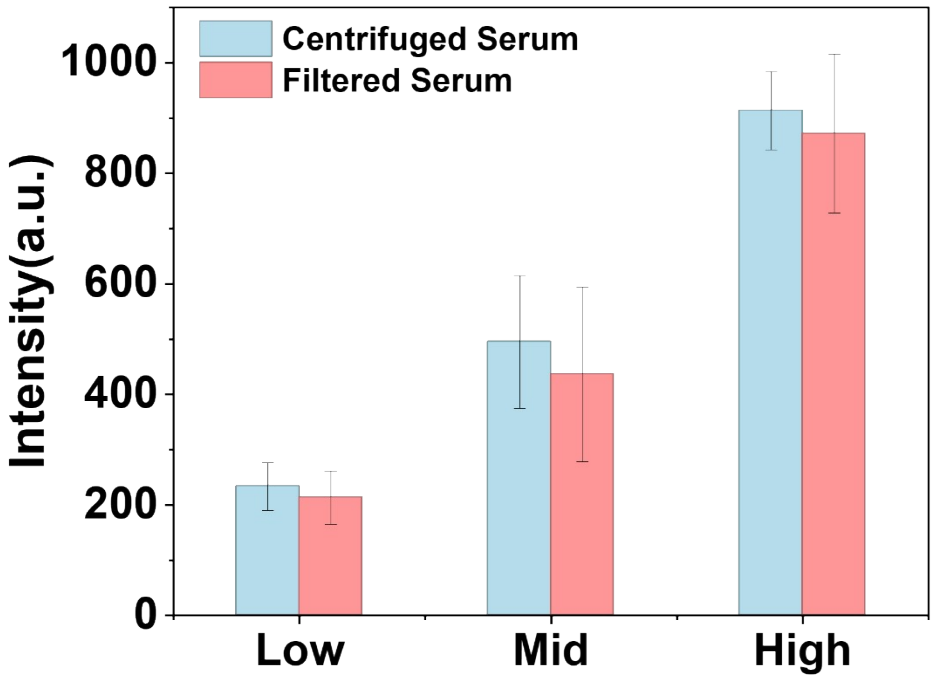

Figure S7. Spike-and-recovery test for membrane filtration efficiency

Healthy whole blood samples were spiked with patient serum containing known concentrations of alpha-fetoprotein (AFP) to achieve final nominal concentrations of 1.4 $ng \cdot mL^{-1}$ (low), 11.58 $ng \cdot mL^{-1}$ (mid), and 137.38 $ng \cdot mL^{-1}$ (high). Each spiked sample was processed through the on-chip membrane filtration device, and the recovered serum was collected. The AFP concentration in the filtrate was measured using the photonic crystal microarray assay. Recovery rates were calculated as the ratio of the measured concentration to the spiked concentration. Across all three levels, the recovery ranged from 85% to 95%, indicating acceptable analyte recovery with minimal nonspecific adsorption to the filtration membrane.

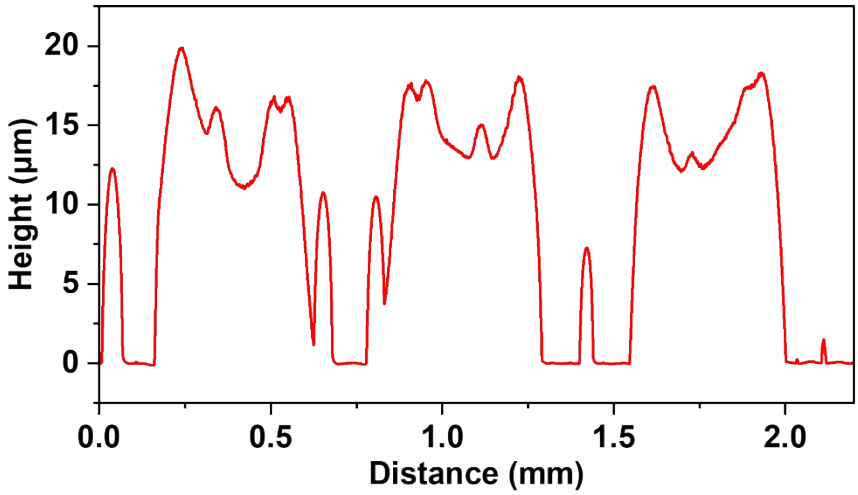

Figure S8. Cross-sectional profilometry of the photonic crystal region in the integrated microfluidic chip.

Cross-sectional profilometry profile across the photonic crystal region in the integrated microfluidic chip, indicating a colloidal photonic crystal layer thickness of approximately 10 µm

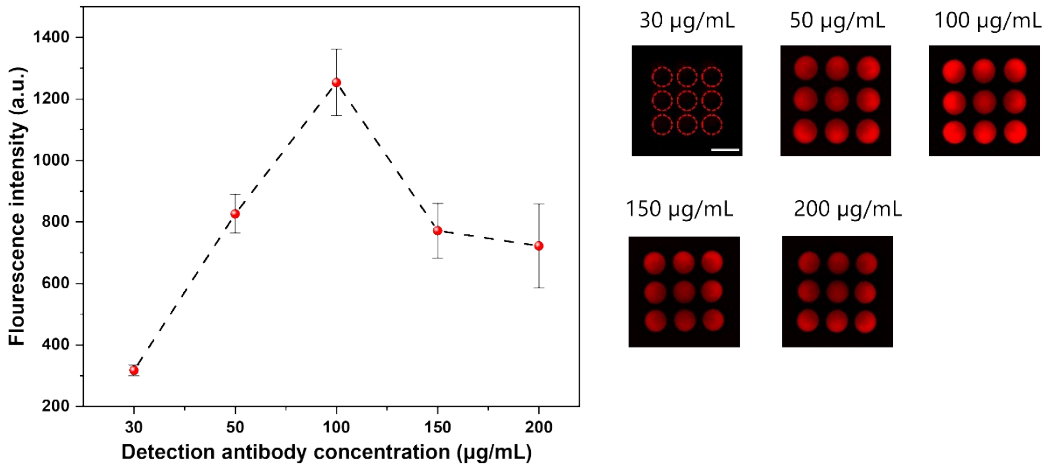

Figure S9. Effect of Cy5-dAb concentration on the fluorescence signal ratio for Alpha-fetoprotein (278 pg/mL).(a) Line plot showing the fluorescence signal ratio as a function of Cy5-dAb concentration. (b) Fluorescence images of the photonic crystal biochips at different Cy5-dAb concentrations.

The results indicate that the signal ratio changes with antibody concentration, allowing identification of the optimal Cy5-dAb concentration for sensitive AFP detection.

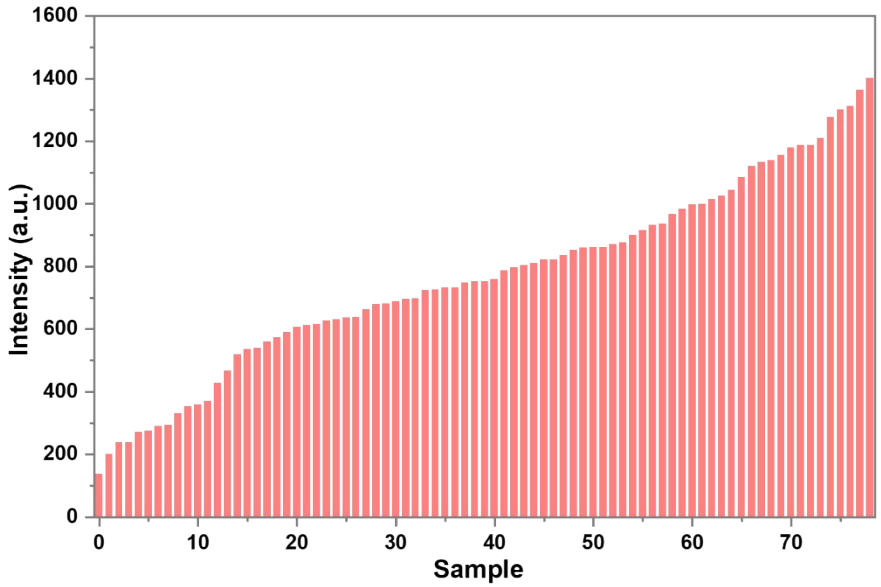

Figure S10. Results from photonic crystal chip assays of clinical samples

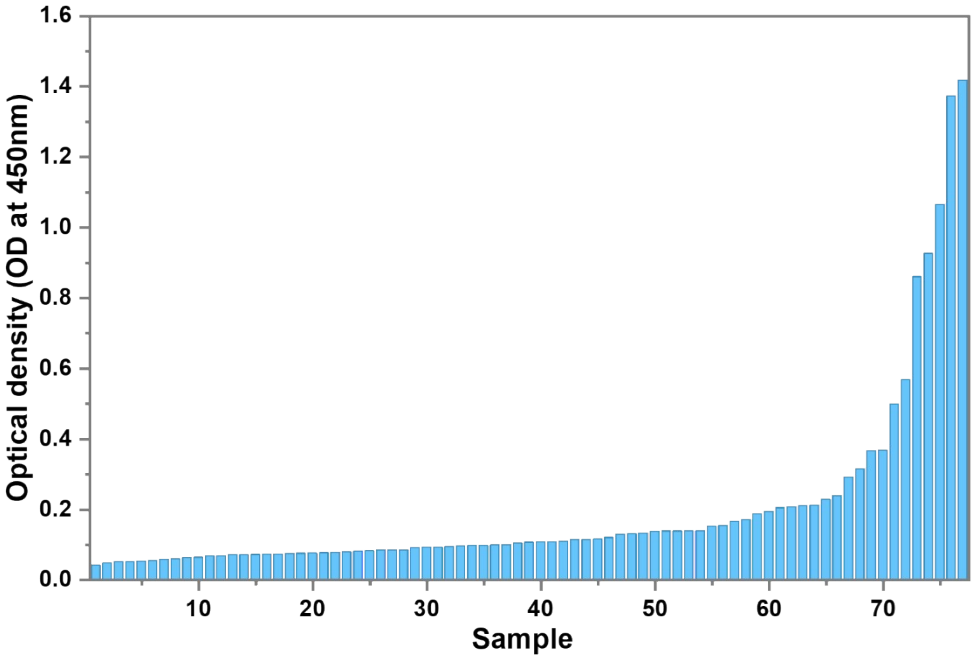

Figure S11. Results from photonic crystal chip assays of clinical samples

Comparison of AFP concentrations measured by the PC microarray and ELISA for each clinical sample (n = 70). Raw signals were converted to concentrations using the respective standard curves.

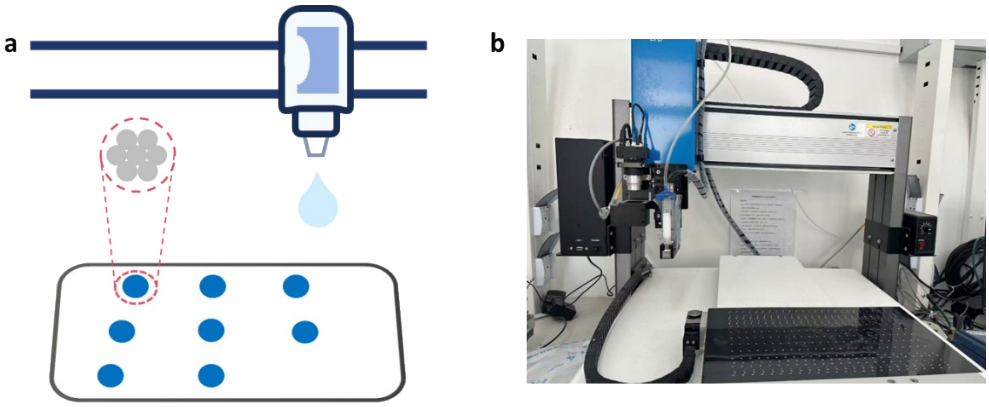

Figure S12 Inkjet printing setup for photonic crystal chip fabrication. (a) Schematic illustration of the inkjet printing process; (b) Photograph of the inkjet printing device.

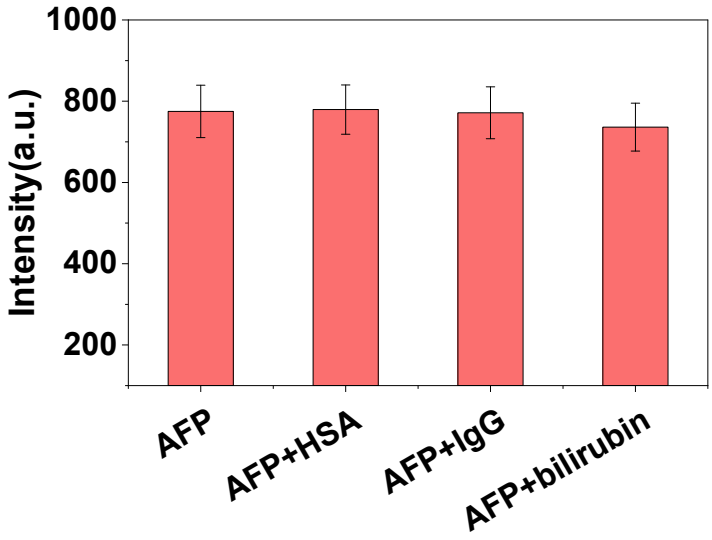

Figure S13. Specificity test of the AFP assay in the presence of HSA (40 mg·mL^{-1}), IgG (15 mg·mL^{-1}), and bilirubin (342 μmol·L^{-1})

Detection method	LOD ($ng \cdot mL^{-1}$)	Dynamic range ($ng \cdot mL^{-1}$)	Assay time	Equipment dependence	Representative reference
Photoelectrochemical aptasensor	0.53	0.001–500	—	High	[1]
Electrochemical aptasensor (AuNPs-MXene)	0.05	1–300	—	High	[2]
Electrochemical aptasensor (PEI-AuNPs)	0.0095	0.01–50	—	High	[3]
Electrochemical immunosensor (paper-based)	0.00062	0.005–50	—	Low	[4]
Microfluidic LIF immunoassay	0.8	1–500	~15 min	High	[5]
Microfluidic electrochemical immunosensor	0.045×10^{-6}	0.0001–200	—	High	[6]
Conventional ELISA (sandwich, nanobody)	0.237	—	~1–4 h	High	[7]
Conventional ELISA (commercial kit)	0.44	—	~1 h	High	[8]
This work	**0.1**	**1–1600**	**~15 min**	**Low**	—

Table S1. Comparison of representative AFP detection methods.

References

1. Y. Wang, T. Jing, H. Qi, Y. Zhao, S. Wan and J. Li, Materials Science in Semiconductor Processing, 2025, 195, 109583.
2. X. Su, J. Chen, S. Wu, Y. Qiu and Y. Pan, Journal, 2024, 24, 7878.
3. P. Yaiwong, S. Anuthum, P. Sangthong, J. Jakmunee, S. Bamrungsap and K. Ounnunkad, 2023, Volume 11 - 2023.

4. C.-W. He, K. Shi, T. Liang, H. Han, L. Chen, X. Guo, J. Chen, K. Li, K. Hao, Y. Cai, N. Hu and Z. Wang, Biosensors and Bioelectronics, 2025, 267, 116821.
5. C. Zheng, P. Dai, H. You, Z. Xian, W. Su, S. Wu, D. Xing and C. Sun, Analytical Sciences, 2024, 40, 1239-1248.
6. J. Zhang, W. Liu, Q. Wang and J. Qu, Electroanalysis, 2023, 35, e202300064.
7. Z. Liao, Q. Zhou and B. Gao, Journal, 2023, 13, 276.
8. B. Su, Y. Wang, H. Pei, Z. Sun, H. Cao, C. Zhang, Q. Chen and X. Liu, Analytical Methods, 2020, 12, 4742-4748.